MRI-Compatible Electromagnetic Spherical Actuator

Boussad MOUALEK[1], Lamia BELGUERRAS[1], Smail MEZANI[1] and Thierry LUBIN[1]
[1] GREEN, Université de Lorraine, F-54000, Nancy, France, boussad.moualek@univ-lorraine.fr

This paper presents the design and optimization of an iron-less spherical actuator capable of operating in an MRI (magnetic resonance imaging) environment. A coupled electromagnetic-thermal approach is adopted for the actuator design. To reduce optimization time, a electromagnetic model is developed to predict the magnetic field generated by the actuator, while a 1D lumped parameter thermal model (LPTM) is employed to estimate the actuator's heating. These models are validated using finite element analyses. MRI compatibility is ensured through the definition of both electromagnetic and thermal criteria.

Keywords – Iron-free actuator, Spherical topology, MRI compatibility, Analytical model, Finite elements

1. INTRODUCTION

Magnetic Resonance Imaging (MRI) is a non-invasive medical imaging technique that provides high-quality images. It is particularly useful for surgical procedures with real-time image feedback. The benefits of this technique are widely recognized by researchers for robot-assisted surgical interventions [1]. MRI-compatible robotic systems have been developed using ultrasonic and pneumatic actuators [2], which have some drawbacks, such as reduced image quality and poor flexibility while operating.

This work aims to develop a new, more compact, and flexible electromagnetic actuation technology for robot-assisted surgical interventions guided by MRI. A cylindrical actuator rotating around one axis has been studied in [3], it presents very good performances but it has only one Degrees Of Freedom (DOF). We propose in this paper a spherical actuator which can rotate in several directions allowing multiple DOF positioning capabilities.

2. ACTUATOR TOPOLOGY AND MODELING

A simple 2-phase spherical actuator (Figure 1) is proposed. It consists of two perpendicular spherical coils powered simultaneously by 2-phase sinusoidal currents. This generates a rotating magnetic field whose interaction with the static magnetic field B_0 inside the MRI scanner bore leads to electromagnetic torque production.

2.1. Electromagnetic model

The torque produced by the actuator is computed using the Lorenz force that B_0 applies on the current density of the coils. In the geometrical configuration presented in Figure 1, the integration over the external sphere's volume, leads to the following formula of the torque along the x-axis:

$$T = \pi^2 B_0 J_e (R_{e2}^4 - R_{i2}^4)/8 \quad (1)$$

This torque remains constant at any position around the x-axis by imposing a current density in the inner sphere such as:

$$J_i = J_e (R_{e2}^4 - R_{i2}^4)/(R_{e1}^4 - R_{i1}^4) \quad (2)$$

The MRI compatibility (ensuring optimal image quality without artifacts) of the actuator requires that the maximum magnetic field it generates at a distance R_0 from the axis of rotation does not exceed 1 ppm of the static field B_0 [4]. To evaluate this criterion, a 3D model was developed to calculate the magnetic field produced by the actuator. Figure 1 illustrates a spherical coil for which the magnetic field distribution was computed using the Biot-Savart law. In this model, a line current is assumed rather than a volumetric current density. The current I in each turn of the spherical coil corresponds to the total number of ampere-turns in each coil. This model remains accurate as long as the calculations are performed at points far from the coil. This approach was chosen for two main reasons: it allows for rapid analytical calculations, which are essential in an optimization context, and it ensures that the model is primarily used to verify the MRI compatibility of the actuator, i.e., to compute the magnetic field only in an imaging zone located at a sufficient distance from the actuator. The analytical solution derived from this model for a single coil is as follows:

$$B_r = \mu_0 \frac{I}{2\pi} \frac{z}{\rho\sqrt{(R+\rho)^2+z^2}} \left(-K(k) + \frac{R^2+\rho^2+z^2}{(R-\rho)^2+z^2} E(k)\right) \quad (3)$$

$$B_z = \mu_0 \frac{I}{2\pi\sqrt{(R+\rho)^2+z^2}} \left(K(k) + \frac{R^2-\rho^2-z^2}{(R-\rho)^2+z^2} E(k)\right) \quad (4)$$

Where μ_0 is the permeability of free space, k is the elliptic parameter, K(k) is the complete elliptic integral of the first kind, E(k) is the complete elliptic integral of the second kind, R is the average radius of the coil, and ρ is the radius at which the magnetic induction is calculated.

To compute the total field produced by the coils, we superimpose the results obtained from each individual turn.

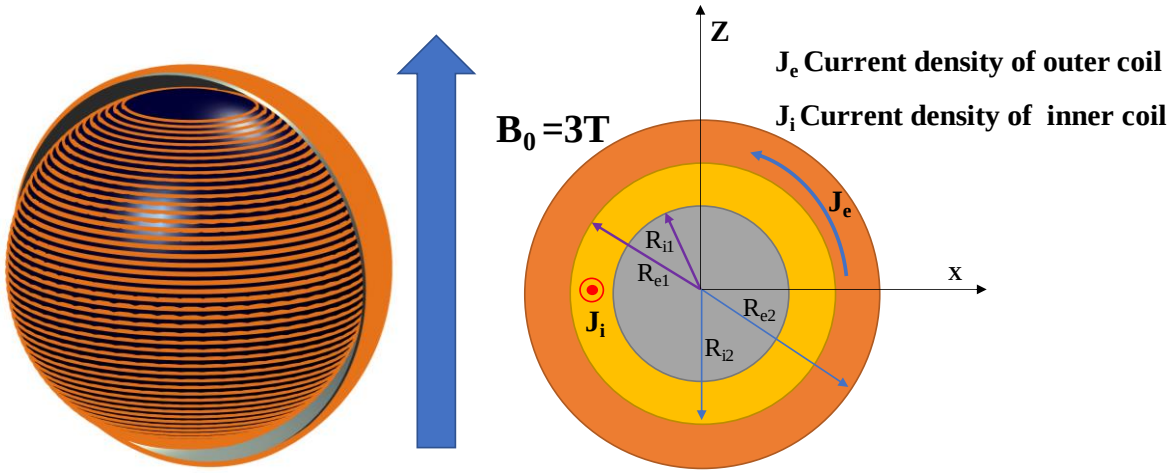

Fig. 1. 2-phase spherical actuator placed in MRI scanner B_0 magnetic field.

A. *Thermal model*

A lumped parameter thermal model (LPTM) is developed to evaluate the actuator heating. Assuming that the heat flows in the radial direction only, a 1D model is used. Each spherical layer is represented by 3 thermal resistances (Figure 2) computed in a similar way as in [5]. The node of mean temperature is connected to a heat source corresponding to the Joule losses generated in the coil.

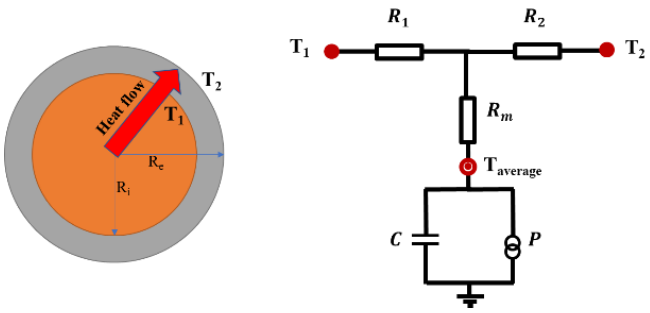

Fig. 2. Elementary block and its equivalent 1D thermal circuit.

The values of the thermal resistances and heat sources are calculated based on the dimensions and losses derived from the electromagnetic model.

$$R_1 = \frac{(-R_i^2 - R_i R_e + 2R_e^2)}{8\pi k R_i\,(R_i^2 + R_i R_e + R_e^2)} \tag{5}$$

$$R_2 = \frac{(-2R_i^2 + R_i R_e + R_e^2)}{8\pi k R_e\,(R_i^2 + R_i R_e + R_e^2)} \tag{6}$$

$$R_m = \frac{3(-R_i^3 - 2R_i^2 R_e + 2R_i R_e^2 + R_e^3)}{40\pi k\;(R_i^2 + R_i R_e + R_e^2)^2} \tag{7}$$

The actuator being surrounded by air, a convective thermal resistance R_c is defined between air and the external and internal actuator's surfaces. For the external surface, R_c is given by:

$$R_c = \frac{1}{4\pi h R_e^2} \tag{8}$$

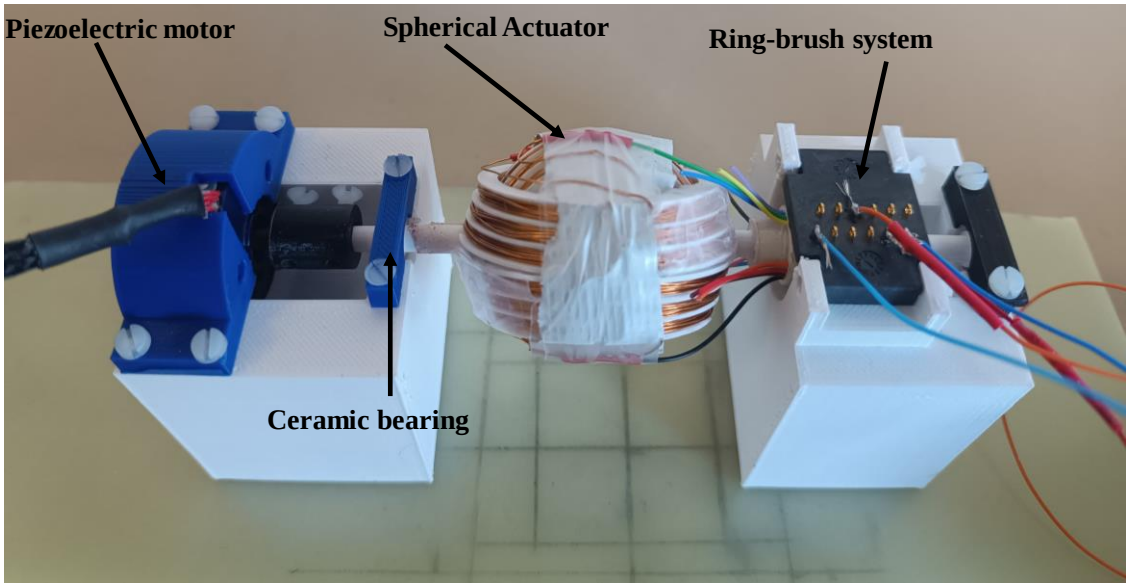

Fig. 3. Spherical Actuator prototype.

3. RÉSULTS AND CONCLUSION

The developed models include two distinct approaches: an electromagnetic model and a thermal model. The electromagnetic model is used to ensure the homogeneity of B0 and to limit the magnetic field generated by the actuator to less than 3 µT. The thermal model is designed to ensure that the actuator's temperature rise remains below 10 °C to comply with patient safety requirements. These two models are coupled and integrated into a constrained optimization algorithm. The objective is to minimize the actuator's volume for a given torque calculated by (1) while satisfying both the electromagnetic and thermal constraints. This optimization process resulted in the following actuator dimensions:

A prototype based on the parameters in Table 1 was developed. Figure 3 shows this prototype, which consists of a spherical actuator, a slip-ring system, ceramic bearings, and a piezoelectric motor used to conduct tests in generator mode. This prototype was optimized and designed to meet the requirements for MRI compatibility.

Tableau 1. Values of parameters derived from the actuator design

Parameters	Optimized values
R (average radius of the inner coil)	20.15 mm
e (winding thickness)	0.8 mm
S_{fils} (wire cross-section)	0.13 mm²
N (number of turns)	72
I (current per turn)	0.182 A

To validate the electromagnetic analytical calculations, a 3D finite element (FE) model was also developed. Since the problem involves an open boundary, the FE model boundary was set at a sufficient distance to impose a zero-vector potential (typically at 20R). Additionally, a dense mesh was used to accurately estimate the magnetic field at R_0, which significantly increased the computational time of the finite element method compared to the analytical model (0.2 s versus 30 s). Figure 4 illustrates the distribution of the magnetic flux density B_z on a spherical surface with a radius of R_0=12 cm [3]. The agreement between the FE and analytical models is excellent. Moreover, the maximum value calculated using the FE method is slightly below 3 µT, thus complying with the constraint on the static field B_0. Finally, the torques calculated analytically and numerically are identical and equal to 71 mNm.

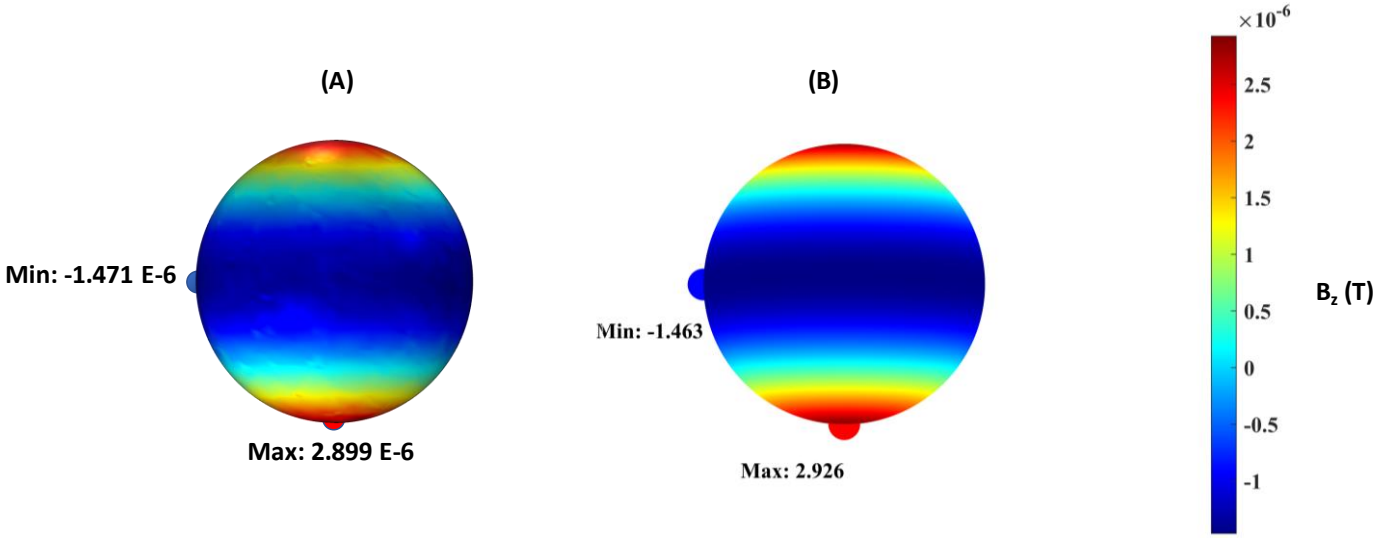

Fig. 4. Magnetic Induction Bz on the Surface of a Sphere with Radius R0 (A: 3D FE Model, B: Analytical Model)

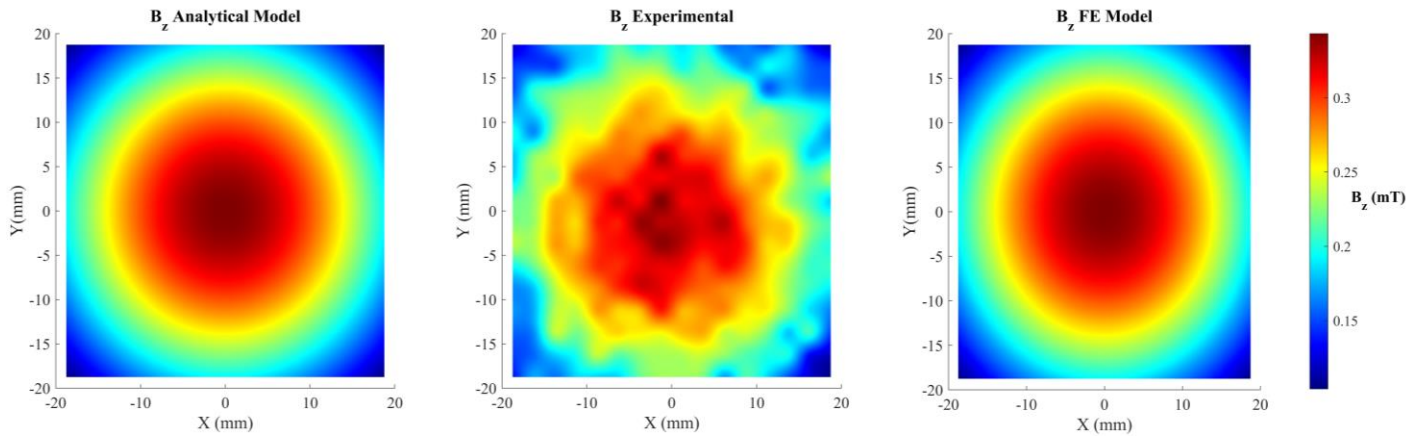

Fig. 5 The comparison between the two models and the measured B_z at a distance of 34.5 mm and I=1A

To validate both models, analytical and FE, magnetic field measurements were performed. Due to limitations related to the measurement equipment, it was not possible to perform the measurements at the distance R_0 and the nominal current, as the range of our probe card exceeds these values. Therefore, the measurements were taken at a distance of 34.5 mm from the center of the actuator along the z-axis, within a square area spanning from −18.75 mm to 18.75mm in both the x and y directions, with a current per coil of I=1 A (to ensure optimal accuracy). Figure 5 shows the comparison between the two models and the measured B_z. The results obtained validate both models, with a maximum B_z measured at 0.35 mT, identical for both models and the experimental measurements.

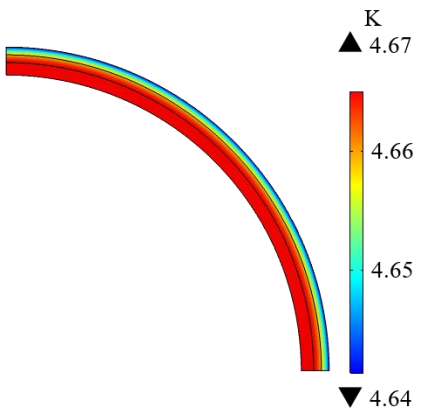

Fig. 6. Steady state temperature-rise distribution using FE analysis.

To validate the LPTM model, a 3D finite element thermal model was also implemented. A good agreement is observed since the steady state average winding temperature-rise calculated with the LPTM is about 4.7°C while the FE model gives 4.67°C (Figure 6). The computation time of the FE is about 20 s which is much higher than the LPTM model which lasts 1 s.

During a sample extraction, the actuator drives a needle (using a lead screw/nut system not shown here) describing an operating cycle in which the rms current I in the actuator varies with time as follows: Start 0-1 s, I=10.I0, steady drive 1-7 s, I=I0, locked in position 7-15 s, I=5.I0, inverse start 15-16 s, I=10.I0, inverse steady drive 16-22 s, I=I0, idle state 22-40 s, I=0. I0 is the rated current of the actuator.

Figure 7 shows the heating of the actuator during 5 cycles. It can be seen that the highest temperature-rise does not exceed 10 °C, making the operation safe in regard to the person's protection against any potential burn. It should be noted that the LTPM and 3D FE models give similar results.

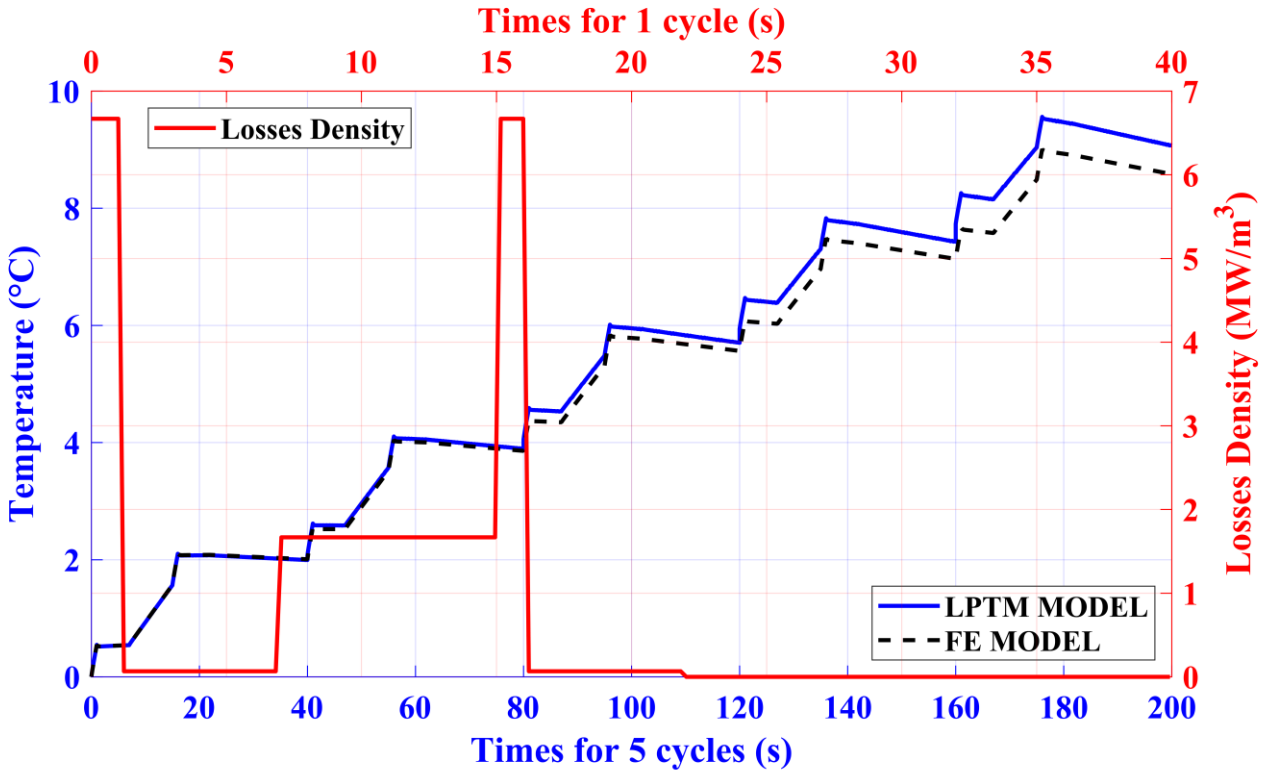

Fig.7. Temperature-rise of the actuator during an operating cycle

4. REFERENCES

[1] R. Gassert, A. Yamamoto, D. Chapuis, et al., “Actuation methods for applications in MR environments,” Concepts Magn. Reson., vol. 29B, no 4, p. 191 209, oct. 2006.

[2] G. S. Fischer, A. Krieger, I. Iordachita, et al., “MRI Compatibility of Robot Actuation Techniques – A Comparative Study,” MICCAI 2008, vol. 5242.

[3] B. Moualek, S. Chauviere, L. Belguerras, S. Mezani, et T. Lubin, “MRI compatible electromagnetic actuator: magneto-thermal design and optimization,” COMPEL, vol. 43, no 3, p. 620 633, jul. 2024,

[4] E. N. Manson, S. Inkoom, A. N. Mumuni, “Impact of Magnetic Field Inhomogeneity on the Quality of Magnetic Resonance Images and Compensation Techniques: A Review,” Reports in Medical Imaging. 2022; 15: 43-5.

[5] P. H. Mellor, D. Roberts, and D. R. Turner, "Lumped parameter thermal model for electrical machines of TEFC design," *IEE Proceedings-B,* vol. 138, no. 5, pp. 205-218. 1991.